JACS
JOURNAL OF THE AMERICAN CHEMICAL SOCIETY
pubs.acs.org/JACS
Article

DNL-17: A Small-Pore Aluminophosphate in ABC-6 Family with 24 Stacking Layers Unraveled by Three-Dimensional Electron Diffraction

Chenyang Nie, Yuanhao Li, Xiaona Liu, Nana Yan, Chao Ma, Jiahui Zhu, Linlin Hao, Peng Guo,* and Zhongmin Liu

Cite This: J. Am. Chem. Soc. 2025, 147, 5440−5448
Read Online
ACCESS | Metrics & More | Article Recommendations | Supporting Information

ABSTRACT: Small-pore aluminophosphate (AlPO) molecular sieves (MSs), particularly those in the ABC-6 family, have gained significant attention for their unique capabilities in selective adsorption and energy storage. However, developing new synthesis strategies for designing AlPOs with three-dimensional (3D) channel systems and determining the structures of nanosized novel AlPO MSs remain challenging tasks. In this study, we introduce a new small-pore AlPO with a 3D channel system, named DNL-17, synthesized by using a diquaternary ammonium compound as an organic structure-directing agent (OSDA). Its crystallographic structure was determined through advanced 3D electron diffraction (ED) techniques and further confirmed by emerging integrated differential phase contrast imaging. DNL-17 exhibits a remarkable 24-layer stacking sequence along the *c*-axis and features a variety of composite building units (CBUs), including *d6r*, *can*, *cha*, and *eri*. Significantly, a combination of 3D ED, theoretical calculations, and solid-state ^{13}C NMR reveals that the employed OSDA adopts distinct conformations to stabilize different cages. This finding highlights a novel strategy for constructing AlPO MSs with diverse cage-based CBUs. Furthermore, DNL-17 demonstrates unique selective adsorption properties, particularly in the separation of *n*-butane and isobutane.

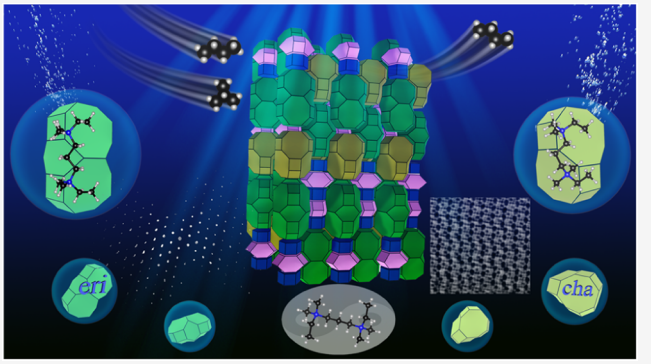

INTRODUCTION

Aluminophosphate (AlPO) molecular sieves (MSs), discovered in 1982 by Union Carbide Corporation, represent a significant class of zeolite-related materials due to their structural versatility and wide-ranging applications in adsorption, separation, and energy storage.[1−4] They are composed of alternating arrangements of AlO_4 and PO_4 tetrahedra, generating various three-dimensional (3D) frameworks with well-defined channels or cavities of molecular dimensions. These AlPO MSs can be categorized into small-, medium-, and large-pore types based on the pore opening delimited by the number of tetrahedra (T). Among these, small-pore AlPO MSs with 8-ring pore openings are particularly noteworthy for their unique capabilities in selective adsorption and energy storage.[5,6] For example, UIO-7 (**ZON**-type AlPO MS) has been used to separate CH_4 and N_2 through a thermodynamic equilibrium separation mechanism.[5,6] The AlPO-42 (**LTA**-type) efficiently stores solar energy through high water uptake and low-temperature regeneration, releasing it as sensible heat via adsorption when needed.[5,6] Furthermore, the incorporation of transition metals or silicon will enrich the chemical composition of the small-pore AlPO family, resulting in the formation of metaloaluminophosphates (MeAlPOs) or silicoaluminophosphates (SAPOs). For example, SAPO-34 with a **CHA** topology has demonstrated remarkable catalytic performance in the methanol-to-olefin (MTO) process, which has been commercialized by our research group.[7,8]

It is worth noting that within the category of small-pore AlPO MSs, the ABC-6 family is particularly dominant. From a structural point of view, they belong to a hexagonal or trigonal crystal system and consist of single 6-rings (*s6r*s) with three distinct positions in the *ab*-plane, denoted as A, B, and C, respectively (Figure 1a). These *s6r*s are stacked along the *c*-axis and further connect through tilted single 4-rings to form a 3D framework, generating structurally diverse cages.[9] Up to now, there are 10 small-pore AlPO MSs within the ABC-6 family. According to the number of *s6r*s stacking layers, the size of

Received: December 19, 2024
Revised: January 17, 2025
Accepted: January 23, 2025
Published: January 31, 2025

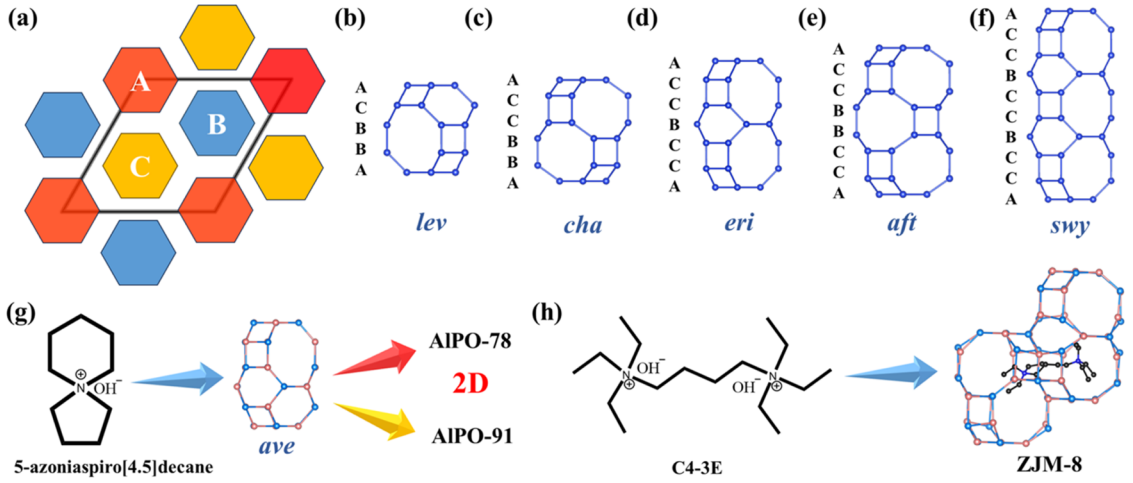

Figure 1. (a) Three different positions of *s6rs* in the ABC-6 family, denoted as A, B, and C. (b–f) The stacking sequence of the commonly seen cages. (g, h) Different synthetic strategies for constructing AlPO-78 and AlPO-91 with two-dimensional (2D) channel systems, as well as ZJM-8 (oxygen atoms were omitted for clarity).

cages from small to large follows this order as shown in Figures 1b–f and S1: *gme*, *lev*, *eab*, *cha*, *ave*, *eri*, *aft*, and *sat* cage.

Although ABC-6 small-pore AlPO MSs with different types of cages have garnered increasing attention, their synthesis remains challenging. One strategy involves using cyclic quaternary ammonium salts as organic structure-directing agents (OSDAs). For instance, the aforementioned **AVE**-type AlPO MS, containing *lev* and *ave* cages, has been synthesized using 5-azoniaspiro[4.5]decane as an OSDA.[10] More interestingly, the secondary OSDA, tetramethylammonium, facilitating the formation of the *gme* cage combined with 5-azoniaspiro[4.5]decane, enables the successful synthesis of a new structurally related AlPO MS (called AlPO-91) with *gme*, *ave*, and *eab* cages.[11] Unfortunately, both small-pore AlPO MSs possess a 2D channel system (Figure 1g). The alternative strategy is utilizing diquaternary ammonium salts as OSDAs. For instance, Alain Tuel et al. synthesized AlPO-17 (**ERI**-type) by using *N*,*N*,*N*′,*N*′-tetramethylhexane-1,6-diamine as OSDA, stabilizing elongated *eri* cages.[12] However, in recent years, only one entirely new structure, ZJM-8 (**JSY**-type), has been reported by Xiao's group by employing triethyl-[4-(triethylazaniumyl)butyl]azanium (denoted as C4–3E) as OSDA.[13] It is worth pointing out that such OSDAs are across through *eri* and *cha* cages and the terminal organic groups stabilize both cages (Figure 1h). To date, there have been a few studies on a single type of diquaternary ammonium salt stabilizing different types of cages, rather than the across-cage strategy observed in ZJM-8.

Beyond the above synthetic hurdles, determining the crystallographic structures of novel AlPO MSs remains challenging, involving the initial framework solution, OSDA locations, and host–guest interactions. This crucial structural information will provide valuable insights into clarifying the role of OSDAs. The primary difficulty lies in the tendency of these materials to crystallize at the nanoscale, which is too small to be investigated using conventional single-crystal X-ray diffraction (SC-XRD). While powder X-ray diffraction (PXRD) can characterize nanocrystals, it compresses 3D data into 1D, complicating the assignment of diffraction intensities to indices and hindering *ab initio* structural determination. Recently, emerging 3D electron diffraction (3D ED) techniques have been proven effective for determining the structures of unknown nanocrystals, including unit cell parameters, space groups, and atomic coordinates.[14–25] Continuous rotation electron diffraction (cRED), a 3D ED technique, stands out for its rapid data collection, minimal radiation damage, and high-quality data, making it invaluable for nanoscale material structural analysis.[4,26–31]

In this article, we report a new member of the ABC-6 family called DNL-17 synthesized by employing ethyl-[3-[ethyl-(dimethyl)azaniumyl]propyl]-dimethylazanium (designated as C3–2M1E) as OSDA. Its crystallographic structure was solved by advanced cRED, revealing that it is a small-pore AlPO MS composed of *d6r*, *can*, *cha*, and *eri* CBUs with a unique 24 stacking layers along the *c*-axis. Combined with the theoretical calculation and solid-state ^{13}C NMR, it indicates that both *eri* and *cha* cages are stabilized by C3–2M1E with distinct conformations. Moreover, it also displays a unique selective adsorption performance in the field of *n*-butane/isobutane separation.

RESULTS AND DISCUSSION

Design and Synthesis of DNL-17. Before exploring the synthesis of small-pore AlPO MS composed of multiple cages in the ABC-6 family, we identified the structural features of commonly observed cages, as shown in Figure 1b–f. Each cage is surrounded by different stacking sequences of single *s6rs* along the *c*-axis. For example, the stacking sequence of *lev* cage is ACBBA (Figure 1b), featuring three 8-rings that create a 2D channel system,[32] while the sequence of the well-known *cha* cage is ACCBBA (Figure 1c). It is worth noting that both *eri* and *cha* cages contain six 8-ring pore openings (Figure 1d). The adjacent 8-ring pore openings in *cha* cages along the *c*-axis are rotated by 60 degrees, whereas those in *eri* cages are not rotated. The 8-ring pore openings in *eri* cages display an elliptical shape, in contrast to the round 8-rings in *cha* cages. Moreover, *aft* and *swy* cages can be considered as expanded versions of *cha* and *eri* cages, respectively (Figure 1e,f). Considering the complexity of *aft* and *swy* cages and 2D channel system resulting from the presence of *lev* cages, in this work, we only focus on the synthesis of small-pore AlPO MS within the ABC-6 family containing *eri* and *cha* cages.

As mentioned in the Introduction section, the utilization of diquaternary ammonium as the OSDA would be a feasible

https://doi.org/10.1021/jacs.4c18190
J. Am. Chem. Soc. 2025, 147, 5440–5448

Scheme 1. Design and Synthesis Scheme of DNL-17[a]

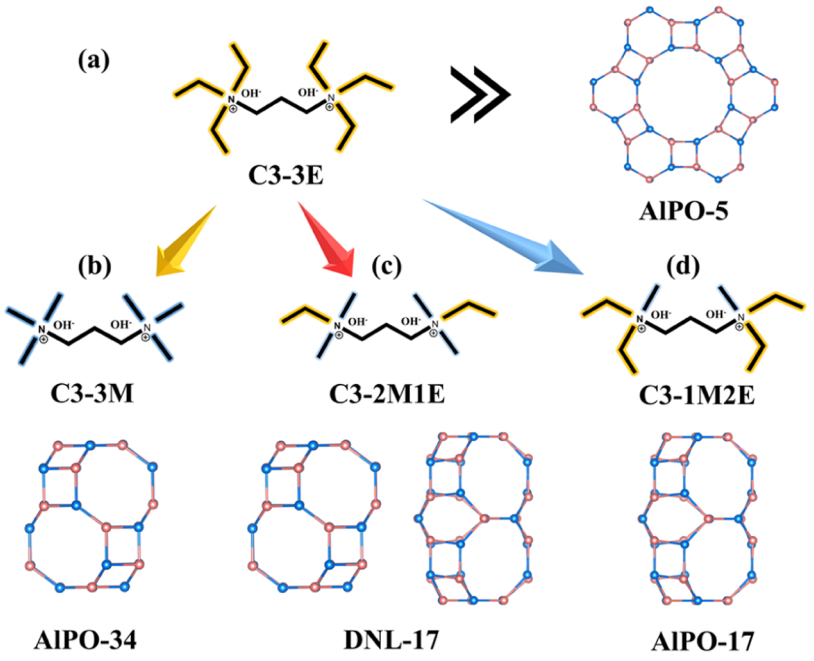

[a]The OSDAs, their abbreviations, and the resulting MS products are shown, with the terminal methyl and ethyl groups highlighted in blue and yellow, respectively.

solution for synthesizing ABC-6 small-pore AlPO MSs. Therefore, the flexible diquaternary ammonium salt as an OSDA was expected to adopt different conformations for directing different cages during the synthesis process. In this case, the length of diquaternary ammonium and size of terminal groups are two important parameters. In the previous work reported by Xiao's group, C4−3E was utilized as the OSDA stabilizing both *eri* and *cha* cages through the across-cage strategy (Figure 1h). It also indicates that neither *eri* nor *cha* cages can accommodate such a large OSDA. Thus, the first attempt was to shorten the length of C4−3E (C4 to C3) and keep the terminal organic groups, resulting in C3−3E (displayed in Scheme 1a) as an OSDA for the following explorations. Based on the empirical chemical gel 1OSDA:0.2HF:1P_2O_5:1Al_2O_3:30TEG:5H_2O, it turns out that the final product is **AFI**-type AlPO-5 (Table 1). It indicates that this OSDA is prone to direct the channel-based framework rather than the caged-based. It is highly possible that the terminal organic groups are slightly too large to be accommodated in the *cha* or *eri* cages.

Table 1. Syntheses from Chemical Gel Composition 1OSDA:*x*HF:1P_2O_5:1Al_2O_3:30TEG: 5H_2O at 200 °C for 72 h

OSDA	HF	products[a]
C3−3M	0.2	AlPO-34 + L[b]
C3−2M1E	0.2	DNL-17
C3−1M2E	0.2	AlPO-17
C3−3E	0.2	AlPO-5
C3−2M1E	0	DNL-17

[a]The phase appearing first is dominant. [b]L stands for layered phase.

The second attempt is to reduce the size of the terminal organic group by replacing ethyl groups with the methyl ones (denoted as C3−3 M as shown in Scheme 1b) for further investigations. Using the identical recipe, the main phase was **CHA**-type AlPO-34 with a triclinic crystal system, accompanied by the unidentified impurity (Table 1). This indicates that the length of C3−3 M is suitable for stabilizing the *cha* cages. Therefore, in the third attempt, the length of the OSDA, C3 backbone, was kept, and then the size of the terminal groups slightly increased, resulting in the selection of C3−1M2E and C3−2M1E for the subsequent exploration. Therefore, we synthesized C3−1M2E and C3−2M1E as OSDAs for exploring new AlPO MS with distinct cages (Scheme 1c,d and Figure S2). The synthesis attempt is still based on the aforementioned recipes 1OSDA:0.2HF:1-P_2O_5:1Al_2O_3:30TEG:5H_2O. It turns out that C3−1M2E can direct the known **ERI**-type AlPO-17, while C3−2M1E can guide the successful synthesis of a new AlPO MS called DNL-17 (Figure S3). Based on these findings, we further adjusted the gel formula of DNL-17 and made attempts to synthesize AlPO and SAPO materials devoid of fluorine (Table S1). The following structural investigations were focused on the AlPO form of DNL-17 synthesized in the absence of fluorine.

Structure Determination of DNL-17-cal and Directing Mechanism of OSDA. After high-temperature calcination at 600 °C, the calcined DNL-17 (DNL-17-cal) shows good crystallinity and its Ar adsorption isotherm result displays that the pore width is 4.3 Å, which indicates that it is a typical microporous MS (Figures S4−S6). The SEM image shows that the DNL-17-cal crystallizes in a nanosized block morphology (Figure S7), and its crystallographic structure cannot be solved by conventional SC-XRD. Hence, we utilized the cRED technique to unravel the crystallographic structure of nanosized DNL-17-cal. A high-quality 3D ED dataset of DNL-17-cal was collected within 3 min through the cRED technique, and its reconstructed 3D reciprocal lattice is shown in Figure 2a. Its hexagonal cell parameters can be deduced from 3D ED data as $a = b = 12.6$ Å and $c = 58.8$ Å. Based on the reflection condition, the possible space groups are $R3$, $R\bar{3}$, $R32$, $R3m$, and

https://doi.org/10.1021/jacs.4c18190
J. Am. Chem. Soc. 2025, 147, 5440−5448

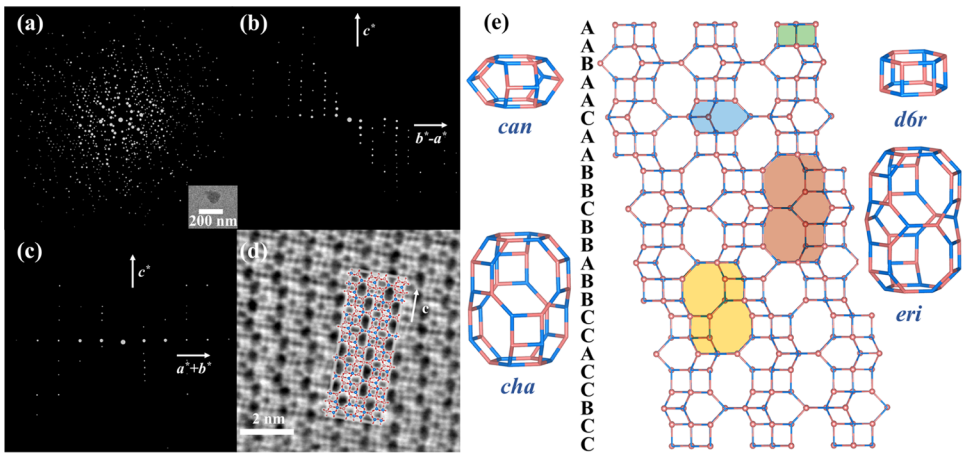

Figure 2. (a) 3D reciprocal lattice of DNL-17-cal. (b, c) 2D reciprocal planes of $hh\bar{1}0l$ and $hh\bar{2}\bar{1}l$. (d) The iDPC image of DNL-17 taken along the [100] direction. (e) The crystallographic structure of DNL-17-cal and different types of cages in DNL-17-cal.

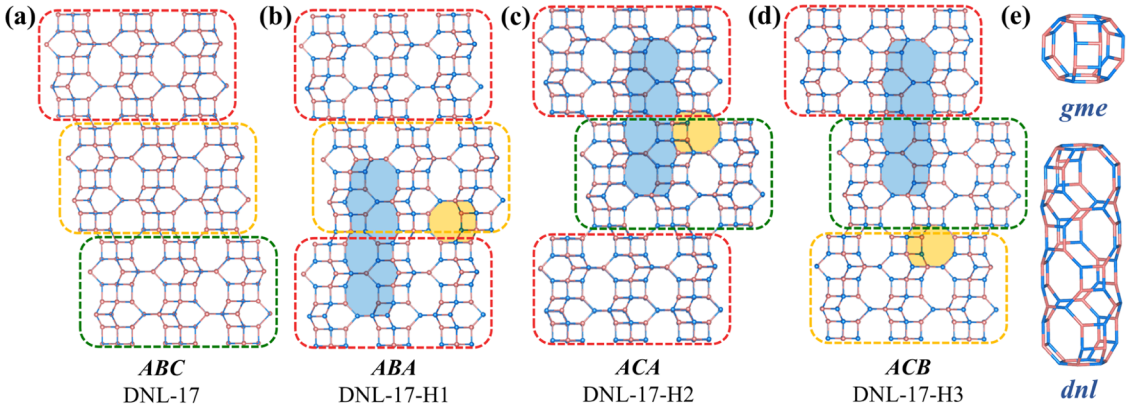

Figure 3. (a–d) The structure of DNL-17-cal and three hypothetical structures (the three arrangements of the DNL-17-layer are marked with red, yellow, and green dotted lines, respectively). (e) Cages different from DNL-17-cal in hypothetical structures.

$R\bar{3}m$ (Figure 2b,c). The initial structural model of DNL-17-cal was solved using direct methods implemented in SHELXT based on *hkl* intensities extracted by XDS[33] with the space group $R\bar{3}$. It turns out that there are 4 aluminum (Al), 4 phosphorus (P), and 16 oxygen (O) atoms in the asymmetric unit identified (Tables S2 and S3). In this case, its chemical composition within one unit cell is $Al_{72}P_{72}O_{288}$. It is significant to note that *can*, *d6r*, *cha*, and *eri* CBUs can be identified in the DNL-17-cal, with only *cha* and *eri* cages featuring accessible 8-rings (Figure 2e). Each *cha* cage is connected to six *eri* cages through shared 8-rings, while each *eri* cage is linked to three *eri* cages and three *cha* cages via shared 8-rings, resulting in a 3D channel system with 8 × 8 × 8-ring pore openings. Moreover, there are nine cages within one unit cell of DNL-17-cal, in which the ratio of *eri* cages to *cha* cages is 2:1. More interestingly, DNL-17-cal belongs to the ABC-6 family, featuring a striking 24-layer stacking sequence of AABAA-CAABBCBBABBCCACCBCC (A) along the *c*-axis. Alongside AlPO-78, DNL-17 represents one of the MSs with the longest stacking sequences in the ABC-6 family. Moreover, the emerging integrated differential phase contrast (iDPC) technique was employed for visualizing the crystallographic structure of DNL-17 along the [100] direction, which is consistent with the one solved by cRED (Figure 2d).

DNL-17-cal can also be considered as the assembly of a thick building layer (denoted as the DNL-17-layer), as shown in Figures 3a and S8. The structure of DNL-17 can be regarded as an *ABC* arrangement of the DNL-17-layers. Based on this structural feature, eight hypothetical structures can be further developed. After excluding the direct connection of two *d6r*s, three structures remain (denoted as DNL-17-H1, DNL-17-H2, and DNL-17-H3), as shown in Figure 3b–d. It is of interest to note that besides *d6r*, *can*, *cha*, and *eri* CBUs, there are two more cages identified in the crystallographic structures of DNL-17-H1 and DNL-17-H2 as shown in Figure 3e. One is the well-known *gme* cage, and the other is an unprecedented cage, currently referred to as the *dnl* cage. The cages with accessible 8-ring pore openings in DNL-17-H3 are limited to the *gme* and *dnl* cages, with no other cages featuring 8-ring apertures. The crystallographic information on these three hypothetical structures are provided in Tables S4–S7.

We also utilized the cRED technique to analyze the structure of as-made DNL-17 (designated as DNL-17-as) for understanding the directing mechanism of such an OSDA (Figure S9), and the important structural information is listed in Tables S8 and S9. It shows that part of Al atoms are 5-coordinated, which is consistent with the solid-state ^{27}Al MAS NMR spectrum (Figure S10). After further structural refinement, the different residual electrostatic potential distributions within *eri* and *cha* cages were observed (Figure S11). However, it is challenging to finalize refinement to locate individual C and N atoms in the OSDA, resulting from the high-symmetry-

https://doi.org/10.1021/jacs.4c18190
J. Am. Chem. Soc. 2025, 147, 5440–5448

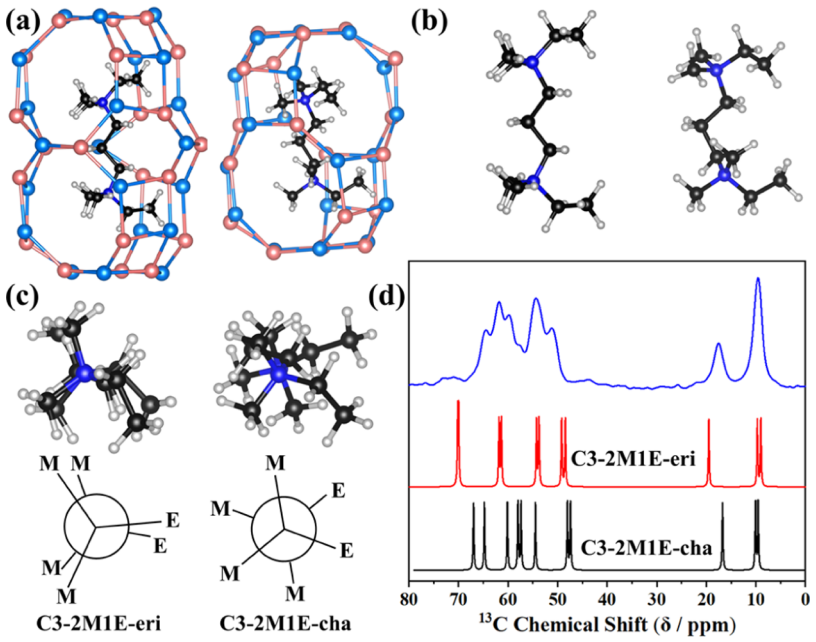

Figure 4. (a) Different conformations of C3−2M1E in *eri* (left) and *cha* (right) cages. (b, c) The front and top views of two conformations of C3−2M1E. (d) Solid-state ^{13}C NMR of DNL-17-as and simulated ^{13}C NMR of two conformations were presented in blue, red, and black, respectively.

induced disorder. The results of the elemental analysis confirm that the OSDA of DNL-17-as did not decompose (Table S10). Moreover, thermogravimetric analysis (TGA) data indicate that either *cha* or *eri* cage in the DNL-17-as is stabilized by one C3−1M2E (Figure S12). Therefore, we carried out a theoretical calculation to determine the locations of OSDAs (Figure S13). After energy optimization, C3−2M1E had different conformations in the *eri* and *cha* cages of DNL-17-as (Figure 4a). Figure 4b,c shows the front and top views of two conformations of C3−2M1E. The two conformations can be clearly distinguished from the top view. If the carbon chain in C3−2M1E is considered as a single bond that can rotate, the C3−2M1E in the *eri* cages can be referred to as the eclipsed conformation, while the C3−2M1E in the *cha* cages can be called the staggered conformation.[34−36] The ^{13}C NMR spectra of the two conformations were simulated through theoretical calculations, and the results were consistent with those of DNL-17-as (Figure 4d). Therefore, C3−2M1E can guide the synthesis of two kinds of cages with distinct conformations.

Butane Isomer Adsorption and Separation. Due to the small-pore openings identified in DNL-17, it can be utilized for separating light alkane isomers and light alkane/alkene. After preliminary explorations (Figures S14−S16), we have discovered that DNL-17 shows the potential application in the separation of *n*-butane and isobutane. Both *n*-butane and isobutane are essential petrochemical raw materials, utilized in direct applications and as intermediates for the production of other petrochemicals.[37−39] As depicted in Figure 5a, the adsorption capacity of DNL-17 for *n*-butane can reach 1.83 mmol/g at 298 K, and the adsorption capacity of isobutane is only 0.19 mmol/g with an uptake ratio of 9.2. Given the presence of both *cha* and *eri* cages in DNL-17, we further tested AlPO-34 and AlPO-17, which contain only *cha* and *eri* cages, respectively. The results revealed that AlPO-17 exhibited a negligible uptake for both gases, while AlPO-34 demonstrated a higher adsorption capacity for *n*-butane compared to DNL-17 (Figure 5b,c). To better understand the relationship between adsorption performance and pore sizes, high-quality 3D ED data of activated AlPO-34, DNL-17, and AlPO-17 were collected and thoroughly analyzed (Tables S11−S14). The pore openings revealed by 3D ED are presented in Figure S17a−c. A comparison of the pore sizes with the dimensions of isobutane shows that isobutane is too large (4.5 Å × 5.5 Å) to be adsorbed by AlPO-34, DNL-17, and AlPO-17. In contrast, *n*-butane, with dimensions of 3.7 Å × 4.0 Å, can be adsorbed by AlPO-34 but not directly by DNL-17 or AlPO-17. However, DNL-17 demonstrated a significant uptake of *n*-butane during isothermal adsorption. Further 3D ED analysis of *n*-butane-adsorbed DNL-17 revealed a notable expansion of the *cha* cage pores (from 4.5 Å × 2.8 Å to 4.5 Å × 3.1 Å), indicating the structural flexibility of DNL-17 (Figure S17d). Therefore, we propose that *n*-butane can pass through DNL-17 due to its flexible structure, similar to how ITQ-55 with elliptical 8-ring pore openings facilitates the passage of ethylene.[40] The dynamic adsorption performances of DNL-17 and AlPO-34 showed notable differences. Specifically, although the overall adsorption capacities of DNL-17 and AlPO-34 were comparable, the adsorption rate of AlPO-34 was significantly slower (Figure 5d). Finally, we conducted breakthrough experiments for *n*-butane and isobutane with concentrations of 50% each and a total flow rate of 1 mL/min. The results indicate that the retention time of *n*-butane in DNL-17 was 20.3 min/g, compared to 6.4 min/g in AlPO-34 (Figure 5e,f). DNL-17 outperforms AlPO-34 by exhibiting a significantly longer residence time for *n*-butane, primarily attributed to its faster adsorption rate. Consequently, DNL-17, with its notable adsorption capacity, stable regeneration ability (Figure S18), and fluorine-free synthesis, demonstrates a strong potential for practical applications.

CONCLUSIONS

A new small-pore AlPO MS DNL-17 with a 3D channel system, belonging to the ABC-6 family, was successfully synthesized using C3−2M1E as the OSDA and characterized by advanced 3D ED. Structural analysis reveals that it is

https://doi.org/10.1021/jacs.4c18190
J. Am. Chem. Soc. 2025, 147, 5440−5448

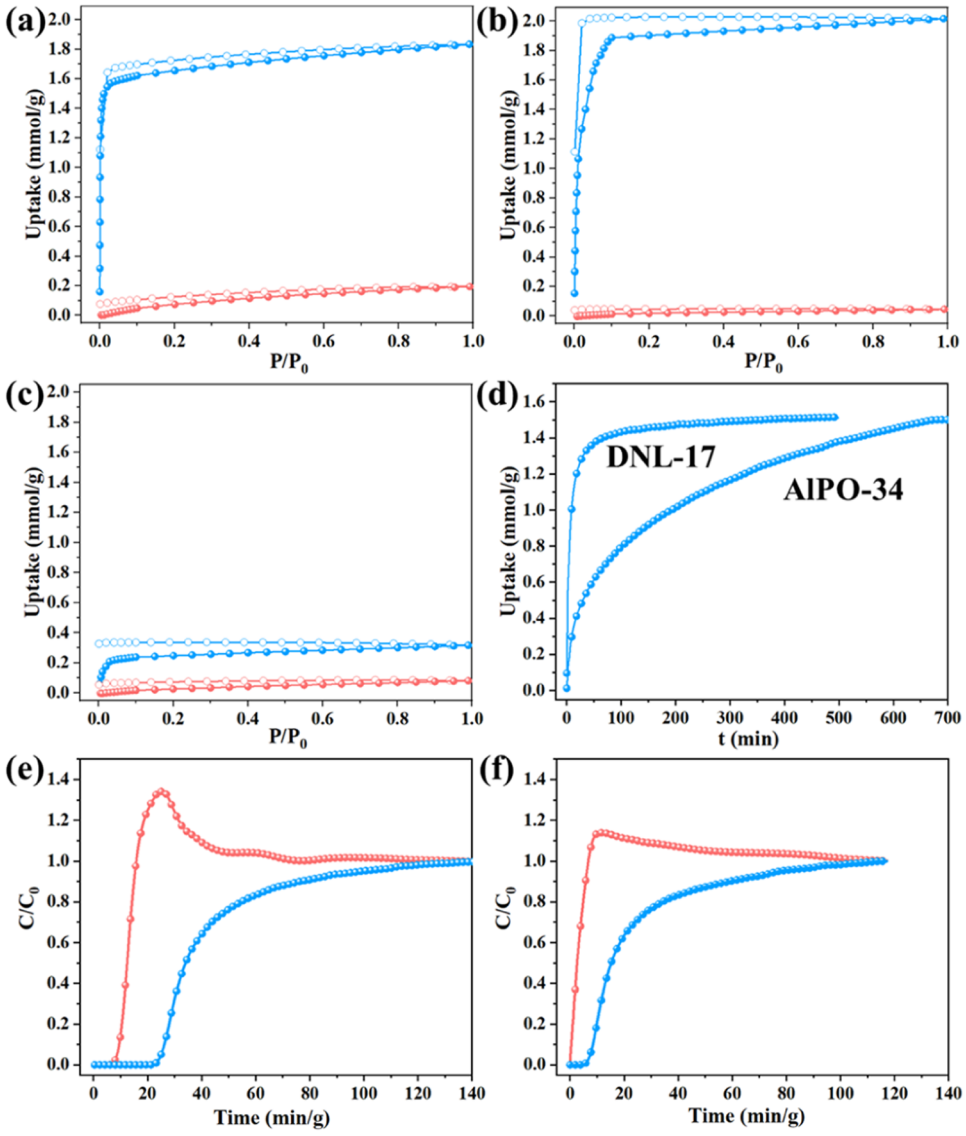

Figure 5. (a–c) *n*-Butane (blue) and isobutane (red) adsorption/desorption isotherms of DNL-17 (a), AlPO-34 (b), and AlPO-17 (c) at 298 K. (d) The dynamic adsorption isotherms of *n*-butane by DNL-17 and AlPO-34 at 298 K and 1 bar. (e, f) Breakthrough experiments of DNL-17 (e) and AlPO-34 (f) for *n*-butane and isobutane at 298 K and 1 bar.

composed of *d6r*, *can*, *cha*, and *eri* CBUs, with a notable 24-layer stacking sequence (AABAACAABBCBBABBC-CACCBCC) along the *c*-axis. Combined with theoretical calculations and solid-state ^{13}C NMR, the stabilization of two key *eri* and *cha* cages by OSDA with distinct conformations has been identified as a unique synthetic strategy. This highlights the potential of flexible OSDAs to unlock new structural diversity, paving the way for the design and synthesis of novel MSs. Additionally, DNL-17 exhibits selective adsorption of *n*-butane over isobutane, making it suitable for the adsorptive separation of isobutane.

EXPERIMENTAL SECTION

Materials. 1,3-Dibromopropane (99%, Aladdin Chemistry Co., Ltd.), trimethylamine solution (30–35%, Aladdin Chemistry Co., Ltd.), triethylamine (99%, Aladdin Chemistry Co., Ltd.), *N*,*N*-dimethylethylamine (99%, Aladdin Chemistry Co., Ltd.), *N*,*N*-diethylmethylamine (99%, Aladdin Chemistry Co., Ltd.), ethanol (99.8%, Aladdin Chemistry Co., Ltd.), hydrochloric acid (HCl, 37%, Kermel), silver oxide (99%, Aladdin Chemistry Co., Ltd.), morpholine (99%, Aladdin Chemistry Co., Ltd.), deuterium oxide (D_2O, 99.9%, Leyan), cyclohexylamine (99%, Aladdin Chemistry Co., Ltd.), aluminum isopropoxide (98%, Aladdin Chemistry Co., Ltd.), phosphoric acid (85%, Damao Chemical Reagent Factory), tetramethoxysilane (98%, Aladdin Chemistry Co., Ltd.), solid silica gel (SiO_2, 98%, Qingdao Haiyang Chemical Reagent), triethylene glycol (98%, Aladdin Chemistry Co., Ltd.), and hydrofluoric acid (40%, Damao Chemical Reagent Factory) were used without further purification. The deionized water was obtained in our laboratory.

Preparation for OSDAs. In a typical synthesis process, 30 g (148.60 mmol) of 1,3-dibromone was dissolved in 150 mL of ethanol, and 24.08 g (356.63 mmol) of *N*,*N*-dimethylethylamine was added dropwise. The resulting mixture was stirred at room temperature for 2 days. It was filtered to recover a white precipitate, washed with ether, and dried to obtain pure ethyl-[3-[ethyl(dimethyl)azaniumyl]propyl]-dimethylazanium; bromide. Subsequently, it was exchanged with silver oxide in the dark to obtain ethyl-[3-[ethyl(dimethyl)-azaniumyl]propyl]-dimethylazanium; dihydroxide (denoted as C3–2M1E).

DNL-17 Synthesis. In a typical synthesis, phosphoric acid was mixed with triethylene glycol (TEG), followed by the addition of aluminum isopropoxide and stirring until uniform. Then, C3–2M1E

https://doi.org/10.1021/jacs.4c18190
J. Am. Chem. Soc. 2025, 147, 5440–5448

and hydrofluoric acid were added to obtain the initial gel mixture, from which water was subsequently evaporated. The final molar composition of the mixture was 1OSDA:0.2HF:1-P_2O_5:1Al_2O_3:30TEG:5H_2O. The mixture was transferred to a stainless-steel high-pressure reactor and crystallized statically at 200 °C for 72 h. After crystallization, the solid product was centrifuged, washed, and dried at 100 °C, yielding a white powder product, DNL-17-as.

AlPO-34 and AlPO-17 Syntheses for Adsorption. The syntheses of AlPO-34 (**CHA**-type) and AlPO-17 (**ERI**-type)[41,42] were carried out as follows: in both cases, phosphoric acid was mixed with water, followed by the addition of aluminum isopropoxide, and stirred to form a uniform mixture. For AlPO-34, morpholine and hydrofluoric acid were added, with a final molar composition of 1.75OSDA:0.5HF:1P_2O_5:0.6Al_2O_3:116H_2O. For AlPO-17, cyclohexylamine and hydrofluoric acid were used, with a final composition of 1OSDA:1HF:1P_2O_5:1Al_2O_3:40H_2O. Both mixtures were transferred to the stainless-steel high-pressure reactor and crystallized statically at 190 °C for 72 h (AlPO-34) or 200 °C for 48 h (AlPO-17), separately. After crystallization, the solid products were centrifuged, washed, and dried at 100 °C to yield the respective white powder products.

Adsorption Measurements. Adsorption/desorption isotherms of *n*-butane and isobutane for all adsorbents were measured by using a Micromeritics 3Flex apparatus at 298 K. Prior to adsorption, DNL-17-cal, AlPO-17, and AlPO-34 were activated at 623 K for 4 h. Dynamic adsorption isotherms of *n*-butane for DNL-17 and AlPO-34 were measured on a BSD-VVS instrument (BEISHIDE Instrument Technology, Beijing) at 298 K and 1 bar, with *n*-butane and N_2 concentrations at 50%. Breakthrough experiments for DNL-17 and AlPO-34 were conducted on a BSD-MAB multicomponent adsorption analyzer (BEISHIDE Instrument Technology, Beijing) at 298 K and 1 bar, with *n*-butane and isobutane concentrations at 50% and a total flow rate of 1 mL/min.

■ ASSOCIATED CONTENT

Supporting Information

The Supporting Information is available free of charge at https://pubs.acs.org/doi/10.1021/jacs.4c18190.

Experimental details include preparation for OSDAs; structural analysis of DNL-17-as; characterizations; and theoretical calculation; and supporting tables and figures (PDF)

Accession Codes

CCDC 2378185 contains the crystallographic data of DNL-17-cal. The data can be obtained for free at https://www.ccdc.cam.ac.uk/data_request/cif through the Internet, or by emailing data_request@ccdc.cam.ac.uk, or by contacting The Cambridge Crystallographic Data Centre, 12 Union Road, Cambridge CB2 1EZ, UK; fax: + 44 1223 336033.

■ AUTHOR INFORMATION

Corresponding Author

Peng Guo − *National Engineering Research Center of Lower-Carbon Catalysis Technology, Dalian Institute of Chemical Physics, Chinese Academy of Sciences, Dalian 116023 Liaoning, China; University of Chinese Academy of Sciences, Beijing 100049, China;* orcid.org/0000-0001-5392-3915; Email: pguo@dicp.ac.cn

Authors

Chenyang Nie − *National Engineering Research Center of Lower-Carbon Catalysis Technology, Dalian Institute of Chemical Physics, Chinese Academy of Sciences, Dalian 116023 Liaoning, China; University of Chinese Academy of Sciences, Beijing 100049, China*

Yuanhao Li − *National Engineering Research Center of Lower-Carbon Catalysis Technology, Dalian Institute of Chemical Physics, Chinese Academy of Sciences, Dalian 116023 Liaoning, China; University of Chinese Academy of Sciences, Beijing 100049, China*

Xiaona Liu − *National Engineering Research Center of Lower-Carbon Catalysis Technology, Dalian Institute of Chemical Physics, Chinese Academy of Sciences, Dalian 116023 Liaoning, China*

Nana Yan − *National Engineering Research Center of Lower-Carbon Catalysis Technology, Dalian Institute of Chemical Physics, Chinese Academy of Sciences, Dalian 116023 Liaoning, China*

Chao Ma − *National Engineering Research Center of Lower-Carbon Catalysis Technology, Dalian Institute of Chemical Physics, Chinese Academy of Sciences, Dalian 116023 Liaoning, China*

Jiahui Zhu − *National Engineering Research Center of Lower-Carbon Catalysis Technology, Dalian Institute of Chemical Physics, Chinese Academy of Sciences, Dalian 116023 Liaoning, China; University of Chinese Academy of Sciences, Beijing 100049, China*

Linlin Hao − *National Engineering Research Center of Lower-Carbon Catalysis Technology, Dalian Institute of Chemical Physics, Chinese Academy of Sciences, Dalian 116023 Liaoning, China*

Zhongmin Liu − *National Engineering Research Center of Lower-Carbon Catalysis Technology, Dalian Institute of Chemical Physics, Chinese Academy of Sciences, Dalian 116023 Liaoning, China; University of Chinese Academy of Sciences, Beijing 100049, China;* orcid.org/0000-0002-7999-2940

Complete contact information is available at: https://pubs.acs.org/10.1021/jacs.4c18190

Author Contributions

The manuscript was written through contributions of all authors. All authors have given approval to the final version of the manuscript.

Notes

The authors declare no competing financial interest.

■ ACKNOWLEDGMENTS

This work was supported by the National Natural Science Foundation of China (Nos. 22288101, 22372156, 22302195, and 22102177).

■ REFERENCES

(1) Wilson, S. T.; Lok, B. M.; Messina, C. A.; Cannan, T. R.; Flanigen, E. M. Aluminophosphate Molecular Sieves: A New Class of Microporous Crystalline Inorganic Solids. *J. Am. Chem. Soc.* **1982**, *104*, 1146−1147.

(2) Fang, W.; Riisager, A. Advances in Aluminophosphates for Catalytic Upgrading of Lignocellulose and Derived Compounds. *ChemCatChem* **2024**, *16*, No. e202400394.

(3) Liu, X.; Yan, N.; Wang, L.; Ma, C.; Guo, P.; Tian, P.; Cao, G.; Liu, Z. Landscape of AlPO-Based Structures and Compositions in the Database of Zeolite Structures. *Microporous Mesoporous Mater.* **2019**, *280*, 105−115.

(4) Nie, C.; Yan, N.; Liao, C.; Ma, C.; Liu, X.; Wang, J.; Li, G.; Guo, P.; Liu, Z. Unraveling a Stable 16-Ring Aluminophosphate DNL-11 through Three-Dimensional Electron Diffraction for Atmospheric Water Harvesting. *J. Am. Chem. Soc.* **2024**, *146*, 10257−10262.

(5) Li, S.; Chen, J.; Wang, Y.; Li, K.; Li, K.; Guo, W.; Zhang, X.; Liu, J.; Tang, X.; Yang, J.; Li, J. Adsorption and Separation of Ch_4/N_2 by Electrically Neutral Skeleton AlPO Molecular Sieves. *Sep. Purif. Technol.* **2022**, *286*, No. 120497.
(6) Krajnc, A.; Varlec, J.; Mazaj, M.; Ristić, A.; Logar, N. Z.; Mali, G. Superior Performance of Microporous Aluminophosphate with LTA Topology in Solar-Energy Storage and Heat Reallocation. *Adv. Energy Mater.* **2017**, *7*, No. 1601815.
(7) Yang, M.; Fan, D.; Wei, Y.; Tian, P.; Liu, Z. Recent Progress in Methanol-to-Olefins (Mto) Catalysts. *Adv. Mater.* **2019**, *31*, No. e1902181.
(8) Tian, P.; Wei, Y.; Ye, M.; Liu, Z. Methanol to Olefins (Mto): From Fundamentals to Commercialization. *ACS Catal.* **2015**, *5*, 1922−1938.
(9) Guo, P.; Yan, N.; Wang, L.; Zou, X. Database Mining of Zeolite Structures. *Cryst. Growth Des.* **2017**, *17*, 6821−6835.
(10) Yuhas, B. D.; Mowat, J. P. S.; Miller, M. A.; Sinkler, W. AlPO-78: A 24-Layer Abc-6 Aluminophosphate Synthesized Using a Simple Structure-Directing Agent. *Chem. Mater.* **2018**, *30*, 582−586.
(11) Yuhas, B. D.; Wilson, K.; Miller, M. A.; Sinkler, W.; Yu, H.; Mowat, J. P. S. AlPO-91: A 16-Layer Abc-6 Aluminophosphate with Five Distinct Cage Types. *ACS Mater. Lett.* **2021**, *3*, 1752−1756.
(12) Tuel, A.; Lorentz, C.; Gramlich, V.; Baerlocher, C. AlPO-Eri, an Aluminophosphate with the Eri Framework Topology: Characterization and Structure of the as-Made and Calcined Rehydrated Forms. *C. R. Chim.* **2005**, *8*, 531−540.
(13) Shi, J.; Hu, J.; Wu, Q.; Chen, W.; Dong, Z.; Zheng, A.; Ma, Y.; Meng, X.; Xiao, F.-S. A Six-Membered Ring Molecular Sieve Achieved by a Reconstruction Route. *J. Am. Chem. Soc.* **2023**, *145*, 7712−7717.
(14) Zhang, D.; Oleynikov, P.; Hovmöller, S.; Zou, X. Collecting 3D Electron Diffraction Data by the Rotation Method. *Z. Kristallogr.* **2010**, *225*, 94−102.
(15) Wan, W.; Sun J Fau - Su, J.; Su J Fau - Hovmöller, S.; Hovmöller S Fau - Zou, X.; Zou, X. Three-Dimensional Rotation Electron Diffraction: Software Red for Automated Data Collection and Data Processing. *J. Appl. Crystallogr.* **2013**, *46*, 1863−1873.
(16) Kolb, U.; Gorelik, T.; Kübel, C.; Otten, M. T.; Hubert, D. Towards Automated Diffraction Tomography: Part I—Data Acquisition. *Ultramicroscopy* **2007**, *107*, 507−513.
(17) Kolb, U.; Gorelik T Fau - Otten, M. T.; Otten, M. T. Towards Automated Diffraction Tomography. Part II–Cell Parameter Determination. *Ultramicroscopy* **2008**, *108*, 763−772.
(18) Kolb, U. A.-O.; Krysiak, Y. A.-O.; Plana-Ruiz, S. Automated Electron Diffraction Tomography - Development and Applications. *Acta Crystallogr., Sect. B:Struct. Sci., Cryst. Eng. Mater.* **2019**, *75*, 463−474.
(19) Smeets, S. A.-O.; Zou, X. A.-O.; Wan, W. A.-O. Serial Electron Crystallography for Structure Determination and Phase Analysis of Nanocrystalline Materials. *J. Appl. Crystallogr.* **2018**, *51*, 1262−1273.
(20) Nannenga, B. L.; Shi, D.; Leslie, A. G. W.; Gonen, T. High-Resolution Structure Determination by Continuous-Rotation Data Collection in Microed. *Nat. Methods* **2014**, *11*, 927−930.
(21) Shi, D.; Nannenga, B. L.; Iadanza, M. G.; Gonen, T. Three-Dimensional Electron Crystallography of Protein Microcrystals. *elife* **2013**, No. e01345.
(22) Palatinus, L.; Corrêa, C. A.; Steciuk, G.; Jacob, D.; Roussel, P.; Boullay, P.; Klementová, M.; Gemmi, M.; Kopeček, J.; Domeneghetti, M. C.; Cámara, F. Structure refinement using precession electron diffraction tomography and dynamical diffraction: theory and implementation. *Acta Crystallogr., Sect. A:Found. Adv.* **2015**, *71* (2), 235−244.
(23) Gemmi, M.; Oleynikov, P. Scanning Reciprocal Space for Solving Unknown Structures: Energy Filtered Diffraction Tomography and Rotation Diffraction Tomography Methods. *Z. Kristallogr. - Cryst. Mater.* **2013**, *228*, 51−58.
(24) Ma, C.; Liu, X.; Nie, C.; Chen, L.; Tian, P.; Xu, H.; Guo, P.; Liu, Z. Applications of X-Ray and Electron Crystallography in Structural Investigations of Zeolites. *Chem. J. Chin. Univ.* **2021**, *42*, 188−200.
(25) Ma, C.; Guo, P.; Liu, Z. DNL-16: A New Zeolitic Layered Silicate Unraveled by Three-Dimensional Electron Diffraction. *Chin. J. Struct.* **2024**, *43*, No. 100235.
(26) Huang, Z.; Willhammar, T.; Zou, X. Three-Dimensional Electron Diffraction for Porous Crystalline Materials: Structural Determination and Beyond. *Chem. Sci.* **2021**, *12*, 1206−1219.
(27) Wang, Y.; Takki, S.; Cheung, O.; Xu, H.; Wan, W.; Öhrström, L.; Inge, A. K. Elucidation of the Elusive Structure and Formula of the Active Pharmaceutical Ingredient Bismuth Subgallate by Continuous Rotation Electron Diffraction. *Chem. Commun.* **2017**, *53*, 7018−7021.
(28) Liu, X.; Liu, L.; Pan, T.; Yan, N.; Dong, X.; Li, Y.; Chen, L.; Tian, P.; Han, Y.; Guo, P.; Liu, Z. The Complex Crystal Structure and Abundant Local Defects of Zeolite EMM-17 Unraveled by Combined Electron Crystallography and Microscopy. *Angew. Chem., Int. Ed.* **2021**, *60*, 24227−24233.
(29) Liu, Y.; Liu, X.; Su, A.; Gong, C.; Chen, S.; Xia, L.; Zhang, C.; Tao, X.; Li, Y.; Li, Y.; Sun, T.; Bu, M.; Shao, W.; Zhao, J.; Li, X.; Peng, Y.; Guo, P.; Han, Y.; Zhu, Y. Revolutionizing the Structural Design and Determination of Covalent−Organic Frameworks: Principles, Methods, and Techniques. *Chem. Soc. Rev.* **2024**, *53*, 502−544.
(30) Ma, C.; Liu, X.; Hong, Y.; Yan, N.; Nie, C.; Wang, J.; Guo, P.; Liu, Z. Fluoride- and Seed-Free Synthesis of Pure-Silica Zeolite Adsorbent and Matrix Using Osda-Mismatch Approach. *J. Am. Chem. Soc.* **2023**, *145*, 24191−24201.
(31) Wang, J.; Ma, C.; Liu, J.; Liu, Y.; Xu, X.; Xie, M.; Wang, H.; Wang, L.; Guo, P.; Liu, Z. Pure Silica with Ordered Silanols for Propylene/Propane Adsorptive Separation Unraveled by Three-Dimensional Electron Diffraction. *J. Am. Chem. Soc.* **2023**, *145*, 6853−6860.
(32) Zhu, G.; Xiao, F.-S.; Qiu, S.; Hun, P.-C.; Xu, R.; Ma, S.; Terasaki, O. Synthesis and Characterization of a New Microporous Aluminophosphate with Levyne Structure in the Presence of Hf. *Microporous Mater.* **1997**, *11*, 269−273.
(33) Kabsch, W. XDS. *Acta Crystallogr., Sect. D:Biol. Crystallogr.* **2010**, *66*, 125−132.
(34) Pophristic, V.; Goodman, L. Hyperconjugation Not Steric Repulsion Leads to the Staggered Structure of Ethane. *Nature* **2001**, *411*, 565−568.
(35) Anderson, J. E.; Casarini, D.; Ijeh, A. I.; Lunazzi, L. Preference for Eclipsed Conformations in Acyclic Neopentyldialkylamines and the Stereodynamical Consequences: An Nmr and Molecular Mechanics Investigation1. *J. Am. Chem. Soc.* **1997**, *119*, 8050−8057.
(36) Papageorgiou, D. G.; Demetropoulos, I. N.; Lagaris, I. E.; Papadimitriou, P. T. How Many Conformers of the 1, 2, 3-Propanetriol Triacetate Are Present in Gas Phase and in Aqueous Solution? *Tetrahedron* **1996**, *52*, 677−686.
(37) Shao, M.; Hu, C.; Xu, X.; Song, Y.; Zhu, Q. Pt/Ts-1 Catalysts: Effect of the Platinum Loading Method on the Dehydrogenation of N-Butane. *Appl. Catal., A* **2021**, *621*, No. 118194.
(38) Liu, J.; Hong, A. S. N. L.; He, N.; Liu, G.; Liang, C.; Zhang, X.; Guo, H. The Crucial Role of Reaction Pressure in the Reaction Paths for I-Butane Conversion over Zn/Hzsm-5. *Chem. Eng. J.* **2013**, *218*, 1−8.
(39) Müller, M.; Kutscherauer, M.; Böcklein, S.; Wehinger, G. D.; Turek, T.; Mestl, G. Modeling the Selective Oxidation of N-Butane to Maleic Anhydride: From Active Site to Industrial Reactor. *Catal. Today* **2022**, *387*, 82−106.
(40) Bereciartua, P. J.; Cantín, Á.; Corma, A.; Jordá, J. L.; Palomino, M.; Rey, F.; Valencia, S.; Corcoran, E. W.; Kortunov, P.; Ravikovitch, P. I.; Burton, A.; Yoon, C.; Wang, Y.; Paur, C.; Guzman, J.; Bishop, A. R.; Casty, G. L. Control of Zeolite Framework Flexibility and Pore Topology for Separation of Ethane and Ethylene. *Science* **2017**, *358*, 1068−1071.
(41) Lohse, U.; Liiffler, E.; Kosche, K.; Jänchen, J.; Parlitz, B. Isomorphous Substitution of Silicon in the Erionite-Like Structure $AlPO_4$-17 and Acidity of SAPO-17. *Zeolites* **1993**, *13*, 549−556.
(42) Marchese, L.; Frache, A.; Gianotti, E.; Martra, G.; Causà, M.; Coluccia, S. Alpo-34 and SAPO-34 Synthesized by Using Morpholine as Templating Agent. Ftir and Ft-Raman Studies of the Host−Guest

https://doi.org/10.1021/jacs.4c18190
J. Am. Chem. Soc. 2025, 147, 5440−5448

and Guest−Guest Interactions within the Zeolitic Framework. *Microporous Mesoporous Mater.* **1999**, *30*, 145−153.

https://doi.org/10.1021/jacs.4c18190
J. Am. Chem. Soc. 2025, 147, 5440−5448